Mathematical modeling of atopic dermatitis reveals "double-switch" mechanisms underlying 4 common disease phenotypes

Elisa Domínguez-Hüttinger, PhD,[a,b] Panayiotis Christodoulides, MEng,[a] Kosuke Miyauchi, PhD,[c] Alan D. Irvine, MD, DSc,[d,e,f] Mariko Okada-Hatakeyama, PhD,[c] Masato Kubo, PhD,[c,g] and Reiko J. Tanaka, PhD[a]

London, United Kingdom, Mexico City, Mexico, Yokohama and Tokyo, Japan, and Dublin, Ireland

GRAPHICAL ABSTRACT

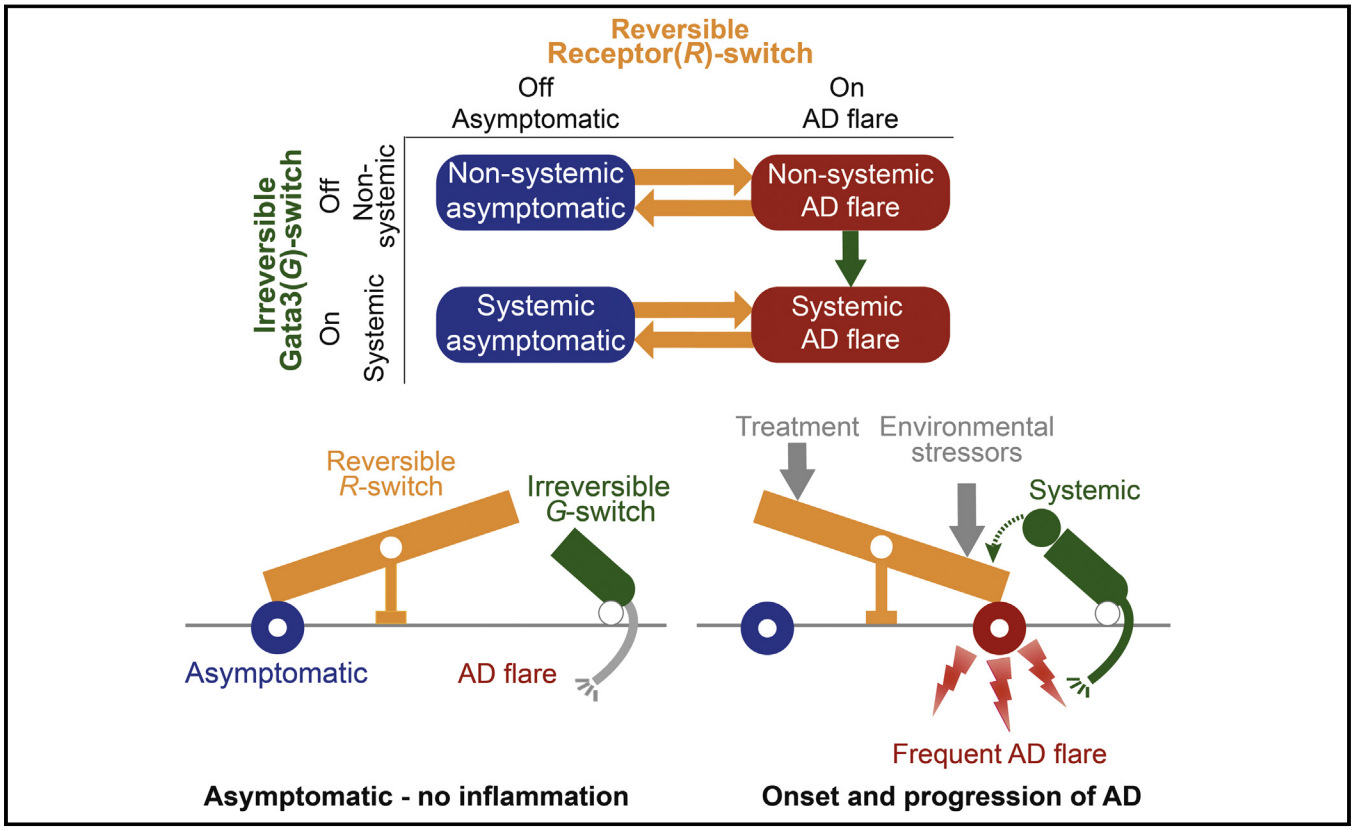

Background: The skin barrier acts as the first line of defense against constant exposure to biological, microbial, physical, and chemical environmental stressors. Dynamic interplay between defects in the skin barrier, dysfunctional immune responses, and environmental stressors are major factors in the development of atopic dermatitis (AD). A systems biology modeling approach

From [a]the Department of Bioengineering, Imperial College London; [b]Instituto de Ecología, Universidad Nacional Autónoma de México, Mexico City; [c]the Center for Integrative Medical Sciences, RIKEN, Yokohama; [d]National Children's Research Centre and [e]Paediatric Dermatology, Our Lady's Children's Hospital Crumlin, Dublin; [f]Clinical Medicine, Trinity College Dublin; and [g]the Research Institute for Biomedical Science, Tokyo University of Science.

Supported by the Engineering and Physical Sciences Research Council of the United Kingdom (EP/G007446/1 to R.J.T.), the Mexican Council for Science and Technology (PhD scholarship 212800 to E.D.-H.), and the National Autonomous University of Mexico (postdoctoral scholarship to E.D.-H.).

Disclosure of potential conflict of interest: E. Domínguez-Hüttinger's institution and she herself have received grants from the Mexican Council for Science and Technology (CONACyT, PhD scholarship 212800), and she has received the RISP travel grant from Riken. A. D. Irvine has received a grant from the National Children's Research Centre. R. J. Tanaka's institution has received a grant from the Engineering and Physical Sciences Research Council, United Kingdom (EG/G007446/1). The rest of the authors declare that they have no relevant conflicts of interest.

Received for publication July 5, 2016; revised October 7, 2016; accepted for publication October 26, 2016.

Available online December 5, 2016.

Corresponding author: Reiko J. Tanaka, PhD, Department of Bioengineering, Imperial College London, London SW7 2AZ, United Kingdom. E-mail: r.tanaka@imperial.ac.uk.

The CrossMark symbol notifies online readers when updates have been made to the article such as errata or minor corrections

0091-6749

© 2016 The Authors. Published by Elsevier Inc. on behalf of the American Academy of Allergy, Asthma & Immunology. This is an open access article under the CC BY license (http://creativecommons.org/licenses/by/4.0/).

http://dx.doi.org/10.1016/j.jaci.2016.10.026

can yield significant insights into these complex and dynamic processes through integration of prior biological data.
Objective: We sought to develop a multiscale mathematical model of AD pathogenesis that describes the dynamic interplay between the skin barrier, environmental stress, and immune dysregulation and use it to achieve a coherent mechanistic understanding of the onset, progression, and prevention of AD.
Methods: We mathematically investigated synergistic effects of known genetic and environmental risk factors on the dynamic onset and progression of the AD phenotype, from a mostly asymptomatic mild phenotype to a severe treatment-resistant form.
Results: Our model analysis identified a "double switch," with 2 concatenated bistable switches, as a key network motif that dictates AD pathogenesis: the first switch is responsible for the reversible onset of inflammation, and the second switch is triggered by long-lasting or frequent activation of the first switch, causing irreversible onset of systemic T_H2 sensitization and worsening of AD symptoms.
Conclusions: Our mathematical analysis of the bistable switch predicts that genetic risk factors decrease the threshold of environmental stressors to trigger systemic T_H2 sensitization. This analysis predicts and explains 4 common clinical AD phenotypes from a mild and reversible phenotype through to severe and recalcitrant disease and provides a mechanistic explanation for clinically demonstrated preventive effects of emollient treatments against development of AD. (J Allergy Clin Immunol 2017;139:1861-72.)

Key words: *Atopic dermatitis, mathematical models, double switch, disease progression, disease phenotypes, preventive treatment*

Abbreviations used
AD: Atopic dermatitis
DC: Dendritic cell
Flg: Filaggrin gene
ft: Flaky tail
NF-κB: Nuclear factor κB
OVA: Ovalbumin
Stat3: Signal transducer and activator of transcription 3
TLR: Toll-like receptor
WT: Wild-type

Atopic dermatitis (AD) is a common chronic skin disease characterized by persistent skin inflammation and a defective skin barrier prone to infections.[1] Although AD affects up to 25% of children worldwide,[2] with a continuous increase in the number of patients and treatment costs,[3] clear guidance and consensus for effective treatment strategies for the prevention and induction of remission are yet to be fully established.[4] The scientific basis for recent clinical recommendations of "proactive therapy" is largely based on clinical trial data with limited duration and scope[5] and waits to be further strengthened by a better understanding of the pathogenic mechanisms of AD. However, a systems-level understanding of AD pathogenesis might lie beyond the ethical and practical reach permitted by clinical and experimental studies and could be supported by a systematic and extensive investigation of the disease dynamics by using mathematical models.[6,7]

Previous studies have identified genetic and environmental risk factors for AD onset, including defects in skin barrier function (the filaggrin gene encoding profilaggrin[8-11] and 30 other putative loci for skin barrier function) and in the immune system, including innate and adaptive immunity.[12-14] In addition, microbiome composition has been shown to play a critical role.[15,16] Each of these risk factors perturbs the system of strongly intertwined regulatory interactions between the keratinocytes (which, along with the extracellular lipids, provide barrier function and also initiate many innate immune responses in the epidermis) and mediators of the adaptive immunity, such as dendritic cells (DCs) and T cells. Perturbations triggered at one part of the system can propagate to another part through interactions, causing synergistic effects of risk factors and a gradual aggravation of the AD phenotype from a mostly asymptomatic mild phenotype at its early stage[17] to a severe treatment-resistant form.[18] Understanding of this dynamic pathogenesis thus requires elucidation of the synergistic effects of multiple risk factors on AD pathogenesis (eg, mutations in skin barrier components accompanied by environmental insults) and the dynamic interplay between the skin barrier, immunity, and the environment, as suggested by several clinical[14,19] and animal or *in vitro* experimental[20-23] studies.

In this study we develop a mathematical *in silico* model of AD pathogenesis that describes the complex and dynamic interplay between skin barrier function, immune responses, and environmental stressors based on clinical and experimental data and our previous model of the early stage of AD.[24] Through systematic and mathematical investigation of the synergistic effects of risk factors on dynamic progression of AD pathogenesis, we tested the hypothesis that genetic risk factors predispose patients to AD progression and decrease the threshold for environmental stressors to drive severe AD.[25] We uncover mechanisms underlying AD onset and progression, explore effective treatment strategies to prevent progression of AD, and answer 3 basic questions about the onset, progression, and prevention of AD: (1) Why do some patients with genetic AD risk factors appear initially asymptomatic but then develop clinically severe AD? (2) Why do some patients progress to severe AD, whereas others maintain mild AD? (3) What are the underlying mechanisms behind effective prevention of AD development by emollients in neonates, as demonstrated in recent clinical trials?[26,27]

METHODS

Model description

The proposed model of AD pathogenesis is described by a hybrid system as follows:

$$\frac{dP(t)}{dt} = P_{\text{env}}\frac{\kappa_{\text{P}}}{1+\gamma_{\text{B}}B(t)} - \alpha_{\text{I}}R(t)P(t) - \delta_{\text{P}}P(t), \tag{1a}$$

$$\frac{dB(t)}{dt} = \kappa_{\text{B}}\frac{1}{1+\gamma_{\text{R}}R(t)}\frac{1}{1+\gamma_{\text{G}}G(t)}(1-B(t)) - \delta_{\text{B}}K(t)B(t), \tag{1b}$$

$$\frac{dD(t)}{dt} = \kappa_{\text{D}}R(t) - \delta_{\text{D}}D(t), \tag{1c}$$

for the dynamics of the 3 variables $P(t)$, $B(t)$, and $D(t)$, denoting the infiltrated pathogen load (in milligrams per milliliter), the strength of barrier integrity (relative to the maximum strength), and the concentration of DCs in the lymph

node (cells per milliliter), respectively. The dynamics of *P(t)*, *B(t)*, and *D(t)* depend on the dynamics of the 3 additional variables *R(t)*, *G(t)*, and *K(t)*, denoting the levels of activated immune receptors, *Gata3* transcription (relative to the maximum transcription level), and active kallikreins, respectively.

The infiltrated pathogen load *(P)* increases by the penetration of environmental stress load *(P_{env})* through the barrier *(B)*. *P* is eradicated by innate immune responses triggered by inflammation *(R)* and is also naturally degraded. The barrier function *(B)* is determined by the balance between its production and degradation. Barrier production is described by a phenomenological representation of its capacity to self-restore nominal barrier function after its disruption and is compromised by innate immune responses triggered by inflammation *(R)* and cytokines produced by differentiated T_H2 cells, levels of which increase according to *G*. The degradation of the barrier occurs as a result of desquamation mediated by active kallikreins *(K)*. The concentration of DCs *(D)* increases while inflammation *(R)* persists but DCs degrade naturally. Equation 1 uses simple mathematical terms based on the law of mass action with zero-order production and first-order degradation terms, except for the barrier production term, $\kappa_x\,(1 - x\,(t))$, which represents the phenomenological recovery of skin barrier in response to disruption.[28] The inhibitory rates are described in the form of $1/(1 + x)$.

The dynamics of *R(t)*, *G(t)*, and *K(t)* is described by a perfect switch as follows:

$$(R(t),\ K(t)) = \begin{cases} \left(R_{off}, K_{off}\right) \text{ if } P(t) < P^- \text{ or } \left\{P^- \le P(t) \le P^+ \text{ and } R\left(t^-\right) = R_{off}\right\} \\ \left(R_{on}, K_{on} = m_{on}P(t) - \beta\right) \text{ if } P(t) > P^+ \text{ or } \left\{P^- \le P(t) \le P^+ \right. \\ \qquad \left. \text{and } R\left(t^-\right) = R_{on}\right\} \end{cases} \tag{2}$$

$$G(t) = \begin{cases} G_{off} \text{ if } D(t) < D^+ \text{ and } G\left(t^-\right) = G_{off} \\ G_{on} \text{ if } D(t) \ge D^+ \text{ or } G\left(t^-\right) = G_{on} \end{cases} \tag{3}$$

where t^- is a time slightly before the time t, as they change abruptly within hours,[29,30] in a much faster time scale than for *P(t)*, *B(t)*, and *D(t)*, which change over weeks.[28,31]

The nominal values of model parameters (Table I)[20,24,28,31-35] were either taken from the previously published model of the early stage of AD,[24] obtained by approximation of the bifurcation diagrams previously derived,[32,33] or derived from the experimental literature.[20,28,31,34,35] Emollient treatments are modeled by adding a constant production term (of 1.5) to the barrier production rate dB/dt.

Model analysis

Model analysis was conducted by using MATLAB (version R2014a; MathWorks, Natick, Mass). We used *ode15s* for numeric integration of the system from steady states as the initial conditions and *output* function to update the switching variables at each step of the iteration. Our model analysis investigated the ranges of $0 \le \alpha_I \le 0.3$ and $0 \le \kappa_P \le 1$. The dynamic trajectories were calculated for 1054 pairs of α_I and κ_P uniformly sampled (an interval of 0.01 for α_I and 0.03 for κ_P). The bifurcation diagram of the proposed model was numerically obtained by using the methodology described in Oyarzún et al[36] to identify the 4 qualitatively different *dynamic phenotypes* with respect to the relative strengths of the feedbacks determined by skin barrier permeability (κ_P) and immune responses (α_I). The steady states for barrier integrity were calculated analytically for the *recovery, bistability,* and *chronic damage* dynamic phenotypes and numerically obtained for the *oscillation* dynamic phenotype by taking the mean of the mean-over-time over the corresponding parameter region for (α_I, κ_P) or by taking the mean for varied levels of skin barrier permeability (κ_P) with an α_I value of 0.25. The basins of attraction for the *bistability* dynamic phenotype for (α_I, κ_P)=(0.04, 0.65) were numerically determined by integrating the system from the points of tangency, (P^-, B^-) and (P^+, B^+), identified by solving $\dot{P}(t) = 0$ at $P(t) = P^-$ and P^+, respectively. The minimal stress load that can trigger systemic T_H2 sensitization were numerically determined by evaluating whether the *D(t)* surpasses the threshold (D^+). The minimal treatment times to achieve remission were numerically determined by evaluating the fold-decrease of P_{env} with which the state (*P(t), B(t)*) enters the healthy basin of attraction. The 95% recovery times were numerically obtained by $t_{95\%} - t_{min}$, where $B(t_{95\%}) = 0.95$ and $B(t_{min})$ is the minimum barrier integrity achieved after a transient AD flare. All the boxplots show the minimum, first quartile, median, third quartile, and maximum values.

Epidermis-specific signal transducer and activator of transcription 3 knockout mice

We developed keratinocyte-specific signal transducer and activator of transcription 3 *(Stat3)* knockout *($Stat3^{f/f}$)* mice with the B6X129 mixed background.[37] All mice used in this study were maintained under pathogen-free conditions. Animal care was conducted in accordance with guidelines of the RIKEN Yokohama Institute.

Development of AD phenotypes in epidermis-specific *Stat3* knockout mice

Expression levels of 11 nuclear factor κB (NF-κB) target genes (*Bcl2*, *Ddx26b*, *Gadd45b*, *Icam1*, *Icam2*, *Icam4*, *Icam5*, *Il1b*, *Tnf*, *Traf1*, *Traf2*, and *Vcam1*) selected from the Kyoto Encyclopedia of Genes and Genomes database (http://www.genome.jp/kegg-bin/show_pathway?ko04064+K02580) were quantified from sorted ear samples of 2-, 5-, 8-, and 10-week-old $Stat3^{f/f}$ mice. By using total RNA isolated with TRIzol, cDNAs were synthesized with the NEBNext Ultra RNA Library Prep Kit for Illumina (New England Biolabs, Ipswich, Mass), according to the manufacturer's instructions. Comprehensive expression analysis was performed by using the mRNA sequence (single-ended 50-bp reads) with the HiSeq 3000 system (Illumina, San Diego, Calif; GEO accession no. GSE86071). Read alignment (mm9) was performed with TopHat2, version 2.0.8, and the expression level was determined with Cufflinks, version 2.1.1, with default settings. We calculated mean expression levels of the NF-κB target genes over the 2 mice per cohort (asymptomatic and AD phenotype) and normalized them by using wild-type (WT) dynamics.

Severity of the AD symptoms was assessed in 11 mice at 51 time points by examining the areas of the skin lesion: no lesions (score 0), periocular lesions (score 1/5), lesions on a half side of the face (score 2/5), on a complete side of the face (score 3/5), on the whole face (score 4/5), or on the whole face and ears (score 5/5). The time of systemic sensitization ($t = 0$) corresponds to the time when the IgE levels increase to 10% of the maximal IgE level measured for each mouse.

RESULTS

Model overview

Our proposed mathematical model of AD pathogenesis (Fig 1, *A* and *B*) is a systems-level representation of the prominent interactions between environmental stressors, skin barrier integrity, and immune responses that were identified based on empiric evidence from numerous clinical[11,20,38-40] and experimental *in vivo*[22,41-45] or *in vitro*[46-48] studies. The model is described by a hybrid system of 3 ordinary differential equations (Equation 1) and includes a double-switch motif with 2 concatenated bistable switches (Equations 2, 3), as detailed below. The first switch is responsible for onset of AD flares, and the second switch is responsible for progression to severe AD. The nominal values of the 21 model parameters were identified from the literature (Table I). This mathematical model includes only the major cellular and biochemical regulators required to describe a global regulatory structure and mechanisms underlying the onset, progression, and prevention of AD rather than explicitly incorporating the fine details of the

TABLE I. Definition of model parameters and their nominal values

Symbol	Name	Nominal value	Reference
P_{env}	Environmental stress load	95 (mg/mL)	24
γ_B	Barrier-mediated inhibition of pathogen infiltration	1	24
κ_P	Nominal skin permeability	0.6 (1/day)	24
α_I	Rate of pathogen eradication by innate immune responses	0.25 (1/day)	24
δ_P	Basal pathogen death rate	1 (1/day)	24
κ_B	Barrier production rate	0.5 (1/day)	24, 28
γ_R	Innate immunity-mediated inhibition of barrier production	10	24
δ_B	Rate of kallikrein-dependent barrier degradation	0.1	24
γ_G	Adaptive immunity-mediated inhibition of barrier production	1	20
κ_D	Rate of DC activation by receptors	4 cells/(mL × day)	31, 34
δ_D	Rate of DC degradation	0.5 (1/day)	35
P^-	Receptor inactivation threshold	26.6 (mg/mL)	32
P^+	Receptor activation threshold	40 (mg/mL)	32
D^+	GATA-3 activation threshold	85 (cells/mL)	34, 33
R_{off}	Receptor off level	0	32
R_{on}	Receptor on level	16.7	32
G_{off}	GATA-3 off level	0	33
G_{on}	GATA-3 on level	1	33
K_{off}	Kallikrein off level	0	32
m_{on}	Slope of the linear relation between $P(t)$ and K_{on}	0.45	32
β_{on}	Y-intercept of the linear relation between $P(t)$ and K_{on}	6.71	32

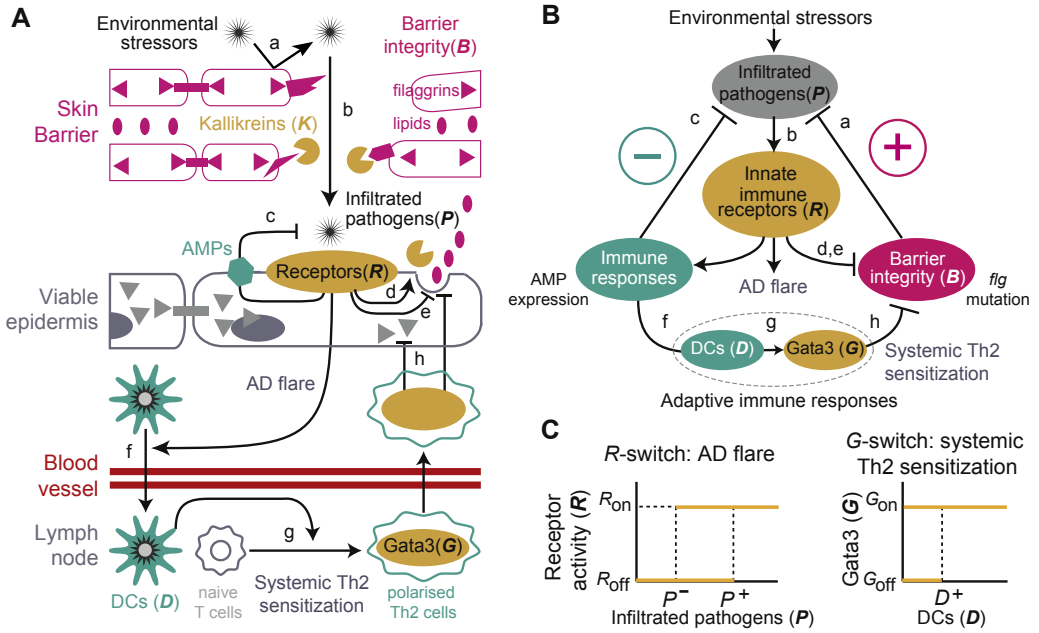

FIG 1. Mechanistic model of AD pathogenesis with a double-switch motif. **A,** Schematic diagram of the processes included in the model. Italics denote the state variables in the model equations (Equation 1). **B,** Control structure of the system regulating AD flares through positive and negative feedback. **C,** *R*-switch (reversible activation of innate immune receptors) and *G*-switch (irreversible GATA-3 transcription).

complex molecular and cellular processes that control epidermal function.

Our model results are validated by clinical and experimental data derived from mouse models with perturbations in either skin barrier function, immune responses, or environmental stressors, the interplay of which is investigated in our model: mouse models with barrier deficiency (flaky tail *[ft]* mice[21,22] with the double mutation involving the filaggrin gene *(Flg)* and *Tmem79*, which encodes lamellar granules,[49] filaggrin null *[Flg*$^{-/-}$*]* mice,[23] and *Tmem79*-deficient mice[50,51]), keratinocyte-specific *Stat3* knockout mice with dysregulated immune responses,[37,52,53] and mouse models in which AD symptoms are induced solely by environmental stressors.[54,55]

A first switch for onset of AD flares

The first part of the model (processes a-e in Fig 1, *A* and *B*, described below) elucidates the mechanisms of how the activity of the first switch (switch-like activation of innate immune receptors) is regulated and leads to AD flares.

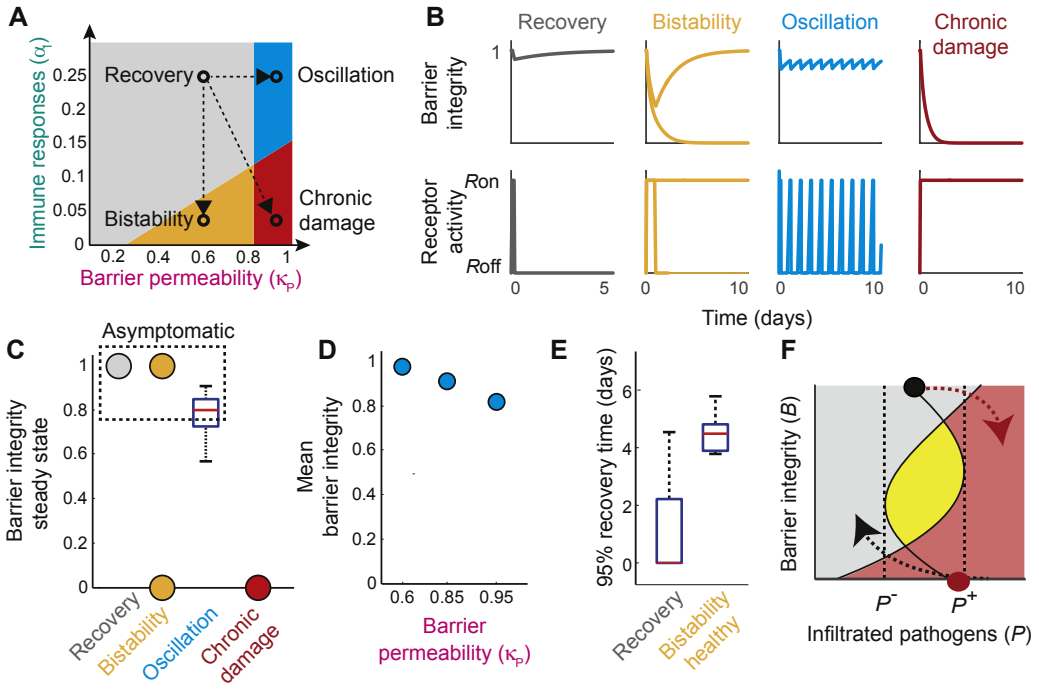

FIG 2. Computationally predicted effects of the 2 main genetic risk factors on the dynamic response to environmental stressors. **A,** Schematic of the bifurcation diagram. The circles in Fig 2, *A*, represent the parameter values used to generate the example dynamics for each of the 4 dynamic phenotypes **(B)**. **C,** Steady states of barrier integrity. **D,** Dose dependency of filaggrin deficiency on mean barrier integrity. **E,** Time required to regain 95% of the healthy steady state of barrier integrity. **F,** Basin of attraction in the (*P, B*)-space. The basins of attraction of the healthy *(black circle)* and unhealthy *(red circle)* steady states are represented by the grey and red regions. The states in the yellow region converge to the healthy steady state if the initial condition is $R = Roff$ and to the unhealthy steady state if the initial condition is $R = Ron$.

Healthy barrier integrity protects the body from environmental stressors (process a) and is maintained by a combination of regulated processing of filaggrin[22] and lipid contents, which constitute lipid envelopes of corneocytes. When barrier integrity is compromised by, for example, excessive skin desquamation through active kallikreins,[41] environmental stressors, including pathogens (eg, *Staphylococcus aureus*),[38] infiltrate the barrier and stress the viable epidermis. They are recognized by innate immune receptors, such as Toll-like receptors (TLRs), which recognize danger-associated molecular patterns and pathogen-associated molecular patterns.[29,47] Activation of the innate immune receptors triggers innate immune responses to eradicate the infiltrated pathogens through release of antimicrobial peptides (process c),[29] further activates kallikreins (process d),[47] interferes with the *de novo* production of skin barrier lipids (process e),[42] and triggers inflammation,[43] resulting in AD flares with increased levels of IL-33,[56] thymic stromal lymphopoietin,[44] and other alarmin cytokines.[57]

Activation of the innate immune receptors is modelled by a reversible bistable switch[32] between the off and on states ($R = R_{off}$ and R_{on}) with the activation (P^+) and inactivation (P^-) thresholds for the amount of environmental stressors, such as pathogen load, that are recognized by the innate immune receptors (Fig 1, *C*, *R*-switch). When the *R*-switch is on, clinical symptoms of AD flares appear as increased inflammation accompanied by decreased barrier integrity. Our model demonstrates that activation of the innate immune receptors and the subsequent onset and resolution of AD flares is mainly regulated by a combination of negative and positive feedbacks through innate immune responses and barrier integrity (Fig 1, *B*). The relative strengths of the feedbacks can be associated with the 2 most prominent genetic risk factors of AD: mutations in the *FLG* gene,[8,9] which results in a higher skin barrier permeability,[23] and a dysregulated expression of innate immune system components,[12] including regulators of antimicrobial peptide expression (eg, TLRs,[58] nucleotide-binding oligomerization domains,[13] and NF-κB[59]), leading to dysfunctional immune responses and a diminished capacity to eradicate the infiltrated pathogens.

Synergetic effects of genetic risk factors and environmental triggers on dynamic phenotypes for AD flares

We investigated the effects of these 2 genetic risk factors in our model by titrating the model parameters that quantify skin barrier permeability (κ_P) and the capacity to eradicate infiltrated pathogens (α_I) in Equation 1. These analyses correspond to examining carriers of different variations of the genetic risk factors and observing how AD can be developed and proceeded in each cohort as a result of the synergistic effects of environmental stressors and the 2 genetic risk factors. Our model analysis revealed the following 4 qualitatively different *dynamic phenotypes* (Fig 2, *A* and *B*) in response to environmental stressors (eg, pathogenic challenges).

When these intrinsic genetic defects do not exist, a quick recovery of the system to the healthy steady state, with homeostatic barrier integrity and no AD flares ($R = R_{off}$), is achieved after a transient decrease in the barrier integrity and transient AD flares

(*recovery* dynamic phenotype); simultaneous existence of these 2 genetic risk factors results in convergence of the system to the unhealthy steady state, corresponding to a chronically decreased barrier integrity and persistent AD flares ($R = R_{on}$), which potentially leads to chronic tissue damages (*chronic damage* dynamic phenotype); genetic defects leading to dysregulated immune responses result in bistability, where wither the healthy or unhealthy steady state is achieved (*bistability* dynamic phenotype); and genetic defects leading to high skin barrier permeability result in persistent oscillatory dynamics caused by the switching of R between R_{on} and R_{off} (*oscillation* dynamic phenotype).

The steady state barrier integrity for the oscillation dynamic phenotype is computationally predicted to be indistinguishable from that of the healthy steady state (Fig 2, *C*), with a slightly lower mean but increased variability. These long-term dynamic behaviors are concordant with a slightly lower but more variable skin barrier integrity observed in *Flg*$^{-/-}$[23] and *ft* mice[21,22] compared with that seen in WT mice. Our model analysis further predicts a gradual decrease in steady state barrier integrity for increased barrier permeability (κ_P), corresponding to the dose-dependent effects of filaggrin deficiency on the severity of AD symptoms (Fig 2, *D*).[9]

The *bistability* dynamic phenotype might also be asymptomatic (or subclinical) if it converges toward the healthy steady state. However, our model analysis demonstrates that the healthy steady state of the *bistability* dynamic phenotype is distinguishable from that of the *recovery* dynamic phenotype based on the much longer time for recovery to regain the same healthy steady state from transient barrier damage (Fig 2, *E*) because of the existence of the second stable (unhealthy) steady state. This model prediction is consistent with the slower skin barrier recovery after tape stripping observed in nonlesional skin of patients with AD compared with healthy subjects[60] and in inflamed compared with noninflamed human skin.[61]

The boundaries of the basins of attraction for the *bistability* dynamic phenotype are computationally obtained by finding the points of tangency between the switching thresholds for the reversible *R*-switch, P^+ and P^-, and the ($P(t)$, $B(t)$)-trajectories on the phase plane (Fig 2, *F*). The system moves from the healthy to the unhealthy steady state if external inputs (eg, environmental aggressors) push the system into the unhealthy basin of attraction. This worsening of the state was observed in *ft* mice,[21-23] as well as in *Stat3* knockout mice, which demonstrated AD symptoms only after challenged with haptens or LPS, an activating ligand of the innate immune receptor TLR4 (see Fig E1 in this article's Online Repository at www.jacionline.org).[62] Likewise, the system can move back to the healthy from the unhealthy steady state if external inputs (eg, treatments) bring the system back to the healthy basin of attraction, achieving remission. Once the remission is induced, maintenance therapy to keep the system in the healthy basin of attraction might achieve control of AD symptoms.[63] This potential switching between the healthy and unhealthy steady states by environmental aggressors or treatments is a distinguished feature of the *bistability* dynamic phenotype and is not observable in the *recovery* and *chronic damage* dynamic phenotypes.

A second switch for progression of AD

The second part of the model (processes f-h in Fig 1, *A* and *B*, as described below) includes the main biochemical and cellular players for the allergy-mediating (T_H2) adaptive immune responses triggered by AD flares and is a systems-level synthesis of several lines of empiric evidence from clinical and experimental studies. Using this model, we elucidated mechanisms behind the progression of AD to establish systemic T_H2 sensitization (including increased levels of IgE, a marker of a T_H2-skewed AD phenotype) and systematically investigated how the duration and frequency of AD flares affect the onset of systemic inflammation, including allergic inflammation.

Activation of innate immune receptors causes AD flares with increased levels of cytokines, including thymic stromal lymphopoietin[44]; alarmins, such as IL-33[56]; and others,[57] which together contribute to activation of DCs in the epidermis.[45] These activated DCs migrate to lymph nodes (process f), where they increase the IL-4 levels[45] and induce expression of *Gata3* (process g),[40] the master transcriptional regulator that controls the irreversible differentiation of naive T cells into T_H2 cells.[45,48] Differentiated T_H2 cells then migrate back to the epidermis, where they contribute to establish an allergic and proinflammatory microenvironment[39] and release cytokines that downregulate the expression of several epidermal terminal differentiation markers, including filaggrin (process h),[20] thereby further compromising barrier integrity.[11] Compromised barrier integrity results in persistent inflammation, even in the absence of additional environmental stressors.

The transcription level of *Gata3* is modelled by an irreversible switch (Fig 1, *C*, *G*-switch)[33]: the transcription remains off ($G = G_{off}$) until sufficient numbers of DCs accumulate in the lymph nodes to reach the activation threshold (D^+), with which transcription initiates ($G = G_{on}$) and persists, even if the DCs disappear ($D = 0$). We assume that *Gata3*-mediated polarization of T cells to T_H2 cells is a hallmark of systemic T_H2 sensitization and that the progression of AD from a mild to more severe phenotype is mediated by this irreversible *G*-switch.

Accordingly, our model of AD pathogenesis suggests that systemic T_H2 sensitization is established if AD flares persist long enough so that $D(t)$ accumulates during the AD flares ($R = R_{on}$) and reaches D^+ to turn on the *G*-switch (Fig 3, *A*, right). AD flares that do not persist long enough do not turn on the *G*-switch because $D(t)$ stays lower than D^+ (Fig 3, *A*, center). Our model analysis predicts that a flare time (t_{on}) of longer than 2.02 days turns on the *G*-switch (Fig 3, *B*, see Equation E5 in this article's Online Repository at www.jacionline.org), which is consistent with experimental observations that the peak of *Gata3* expression is reached in approximately 2 days after *in vitro* stimulation of T_H2 cell differentiation.[48] Systemic T_H2 sensitization is spontaneously established in the *chronic damage* dynamic phenotype because of persistent AD flares and subsequent continuous accumulation of DCs to surpass D^+, turning on the *G*-switch.

Periodic AD flares, as in the *oscillation* dynamic phenotype, are also predicted to turn on the *G*-switch if the relaxation time (t_{off}) between AD flares (when $R = R_{off}$) is too short to prevent a gradual accumulation of DCs that eventually surpass the threshold D^+ (Fig 3, *C*, right). The minimum relaxation time above which the *G*-switch stays off is analytically obtained as a function of the flare time (t_{on}; white line in Fig 3, *D*, obtained by using Equation E6 in this article's Online Repository at www.jacionline.org). For example, the *R*-spikes with a t_{on} of 1 day turns on the *G*-switch if t_{off} is shorter than 0.93 days (Fig 3, *D*, red circle). Our model simulation for *R*-spikes with a t_{on} of 1 day and t_{off} of 0.9 days

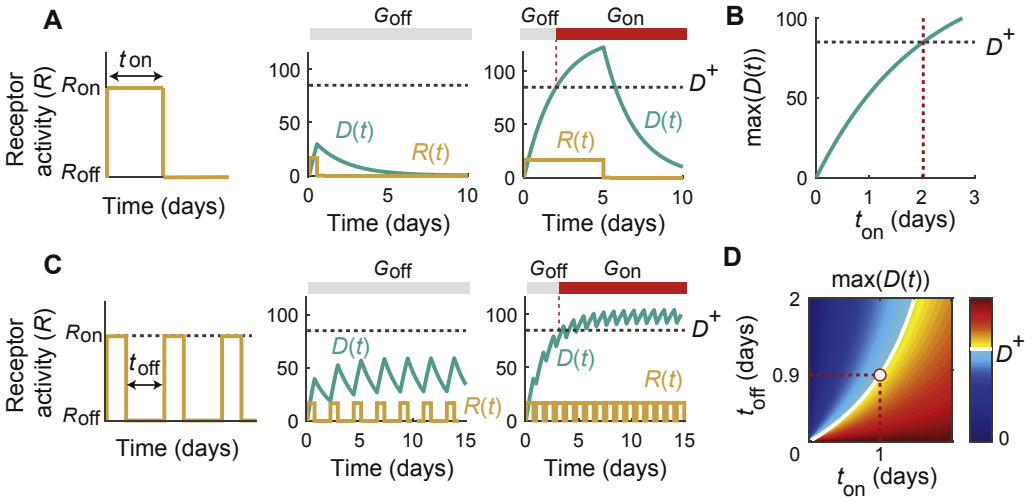

FIG 3. Proposed mechanisms of AD progression through a double switch. The *G*-switch is turned on by accumulation of DCs beyond D^+ because of transient AD flares **(A)** with a flare time (t_{on}) of longer than 2.02 days **(B)** or periodic AD flares **(C)** with a sufficiently small relaxation time (t_{off}) as a function of t_{on} **(D)**.

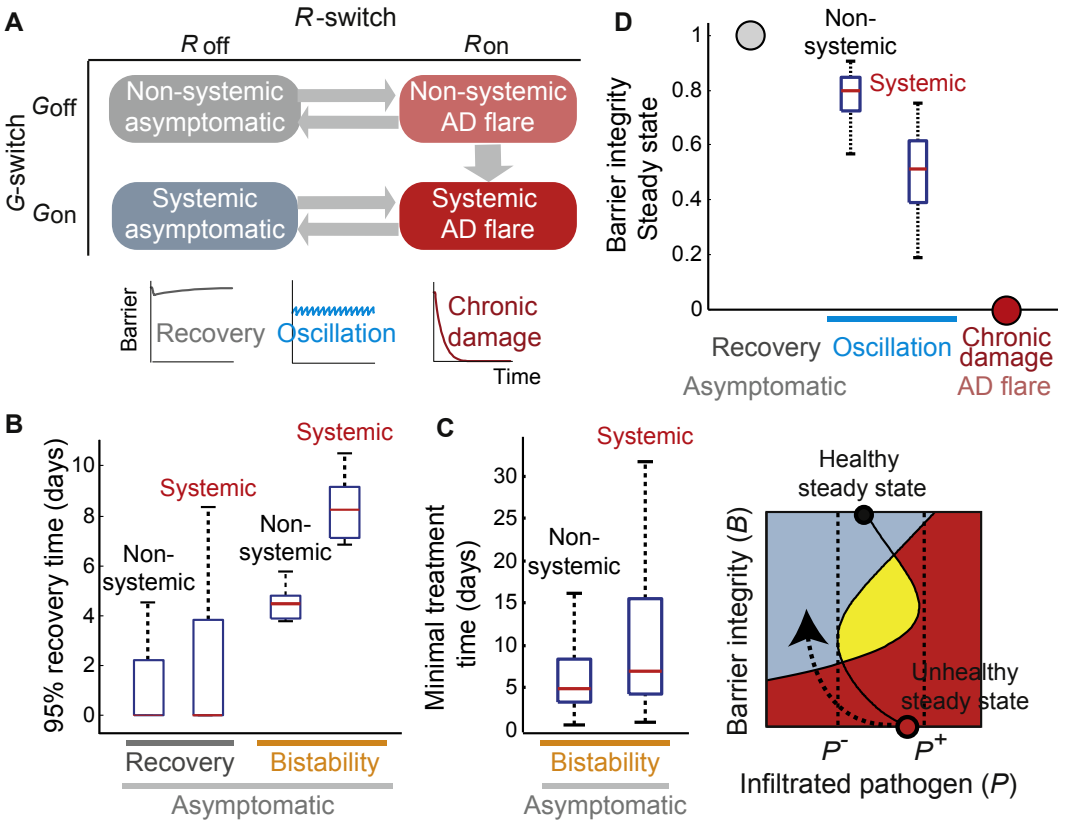

FIG 4. Four AD phenotypes described by the status of the double switch. **A,** The *R*-switch distinguishes between asymptomatic ($R = R_{off}$) and symptomatic ($R = R_{on}$), and the *G*-switch distinguishes between non-systemic ($G = G_{off}$) and systemic ($G = G_{on}$) phenotypes. **B-D,** Systemic phenotypes demonstrate severe AD symptoms compared with non-systemic counterparts, as computationally predicted by a longer 95% recovery time (Fig 4, *B*), longer treatment time required for remission (Fig 4, *C*), and lower barrier integrity (Fig 4, *D*).

predicts turning on of the *G*-switch within 10 days, which is consistent with several features of AD skin, including T_H2 cell infiltration, as observed in mice after repeated application of oxazolone once every other day over 10 days.[55]

Four AD phenotypes classified by a double switch

Taken together, our model of AD pathogenesis is characterized by a double switch with 2 concatenated bistable switches (*R*- and *G*-switches), the status of which represents 4 AD phenotypes of

different severity (Fig 4, *A*). The state of the *R*-switch determines whether the phenotype is asymptomatic ($R = R_{off}$) or symptomatic (AD flare, $R = R_{on}$), and the state of the *G*-switch determines whether it is systemic ($G = G_{on}$) or non-systemic ($G = G_{off}$).

For the symptomatic case, in which the *R*-switch is constantly on and AD flares persist, as in the *chronic damage* or *bistability* (unhealthy) dynamic phenotype, the non-systemic symptomatic (R_{on}, G_{off}) state appears only transiently as it inevitably progresses, after a flare time of $t_{on} = 2.02$ days (Fig 3, *B*), to the (R_{on}, G_{on}) state corresponding to the systemic symptomatic phenotype, the most severe AD phenotype with an impaired barrier integrity, systemic inflammation, and infection.

The asymptomatic case, in which the *R*-switch turns off after a transient AD flare as in the *recovery* or *bistability* (healthy) dynamic phenotype, corresponds to either non-systemic asymptomatic (healthy) phenotype in the (R_{off}, G_{off}) state or systemic asymptomatic phenotype in the (R_{off}, G_{on}) state with subclinical inflammation caused by T_H2-related cytokines. The systemic phenotype demonstrates more severe AD symptoms compared with its non-systemic counterpart, which are computationally characterized by a longer 95% recovery time (Fig 4, *B*). This was suggested by experiments in both WT and $Flg^{-/-}$ mice, which recovered from hapten challenge if unsensitized (non-systemic) but did not recover within 2 days if sensitized (systemic). The more severe symptoms are also computationally reflected by a longer treatment time required for remission (Figs 2, *F*, and 4, *C*) to drive the system from the unhealthy steady state to the healthy basin of attraction for the systemic than non-systemic phenotype because of enlargement of the unhealthy basin of attraction. This prediction is in agreement with the clinical observation that a much higher treatment effort is required to relieve AD symptoms during the chronic phase of AD, which is characterized by high IgE levels (systemic).[17]

The more severe symptoms for the systemic compared with the non-systemic phenotype are also computationally predicted for the case in which *R* is switching between R_{off} and R_{on}, as in the *oscillation* dynamic phenotype, by a decrease in the mean and an increase in the variance of the steady state of the barrier integrity (Fig 4, *D*). This prediction is consistent with the increase in the mean and variance of the transepidermal water loss (an indicator of barrier defects) measured in *ft* mice after induction of systemic T_H2 sensitization.[21]

Genetic risk factors predispose to systemic T_H2 sensitization

Here we use our mathematical model of AD pathogenesis to investigate the synergistic effects of environmental and genetic risk factors on AD progression. Specifically, we calculate the minimum stress load (the strength of the environmental stressors [P_{env}]) that can turn on the *G*-switch by means of its continuous challenge through an AD flare of a single pulse (Fig 5, *A*, left) or of transient oscillation (Fig 5, *A*, right) for different dynamic phenotypes caused by synergetic effects of the genetic risk factors (Fig 2, *A* and *B*). Turning on the *G*-switch (systemic T_H2 sensitization) might appear as a dramatic increase in the severity of AD symptoms, as observed in *ft* and $Flg^{-/-}$ mice on ovalbumin (OVA) challenge.[21,23] The minimum stress load was experimentally evaluated in the dose response in WT mice, in which a systemic AD phenotype was developed through challenges with high (10%) but not lower (≤ 2%) concentrations of *S aureus* in culture supernatants[54] and by 10 repeated, but not single, oxazolone challenges.[55]

Our model simulations predict that the minimum stress load is significantly lower for the *bistability* or *oscillation* dynamic phenotypes that arise in the context of genetic risk factors compared with the *recovery* dynamic phenotype, which is mainly observed when the intrinsic genetic defects do not exist (Fig 5, *B*). This model prediction suggests that genetic risk factors make the patients susceptible to smaller environmental stressors in developing systemic T_H2 sensitization and is concordant with the experimental observation[22] of a low concentration (0.02%) of oxazolone-induced allergic contact dermatitis in *ft* mice but not WT mice and a higher concentration (0.5%) of oxazolone-induced allergic contact dermatitis also in WT mice.

Our predicted increase in the susceptibility to environmental stressors might explain the spontaneous appearance of AD symptoms in some, but not all, carriers of genetic risk factors for AD, as demonstrated in $FLG^{-/-}$ patient cohorts.[8] Carriers of the genetic risk factors who initially appear asymptomatic (as in the *bistability* or *oscillation* dynamic phenotypes; Fig 2, *C*) can demonstrate a sudden and sharp worsening of AD symptoms when they experience systemic T_H2 sensitization, even with naturally occurring (small) fluctuations in the environment (Fig 5, *B*). This observation also implies a possible mechanism behind the dose-dependent effects of filaggrin deficiency on AD symptoms[9] because the *G*-switch is turned on by a smaller environmental load for stronger filaggrin deficiency (Fig 5, *C*).

To test the model-predicted outcome that small and naturally occurring environmental fluctuations can trigger a sudden and sharp worsening of AD symptoms through systemic T_H2 sensitization in carriers of genetic risk factors, we evaluated the temporal changes in AD symptoms for *Stat3* knockout mice in the natural environment with small environmental stressors. Half of the mice had an AD phenotype after 30 weeks, whereas the others remained asymptomatic. Mice that demonstrated an AD phenotype exhibited a much higher expression of the NF-κB target genes (a marker of ubiquitous environmental triggers; Fig 5, *D*),[62] suggesting that naturally occurring environmental triggers contributed to the observed development of the AD phenotype. Together with the observations in *Stat3* knockout mice that a long-lasting exposure to OVA (environmental stressor) triggered a sharp increase in IgE levels (see Fig E2 in this article's Online Repository at www.jacionline.org) and that AD symptoms sharply increased after allergic systemic T_H2 sensitization (increase of IgE; Fig 5, *E*), these experimental results suggest that naturally occurring fluctuations in environmental stressors can trigger systemic T_H2 sensitization in mice with a genetically defective background and worsen their AD symptoms, which is consistent with the model-predicted outcome.

Prevention of AD symptoms by emollient treatments

We further derived the minimum stress load that can turn on the *G*-switch in the presence of continuous application of emollients computationally. The model predictions confirm that emollient treatments, which strengthen barrier integrity and resistance,[64] reduce the susceptibility to environmental stressors in developing systemic T_H2 sensitization in all asymptomatic patient cohorts considered, as demonstrated by a more than 2-fold increase in

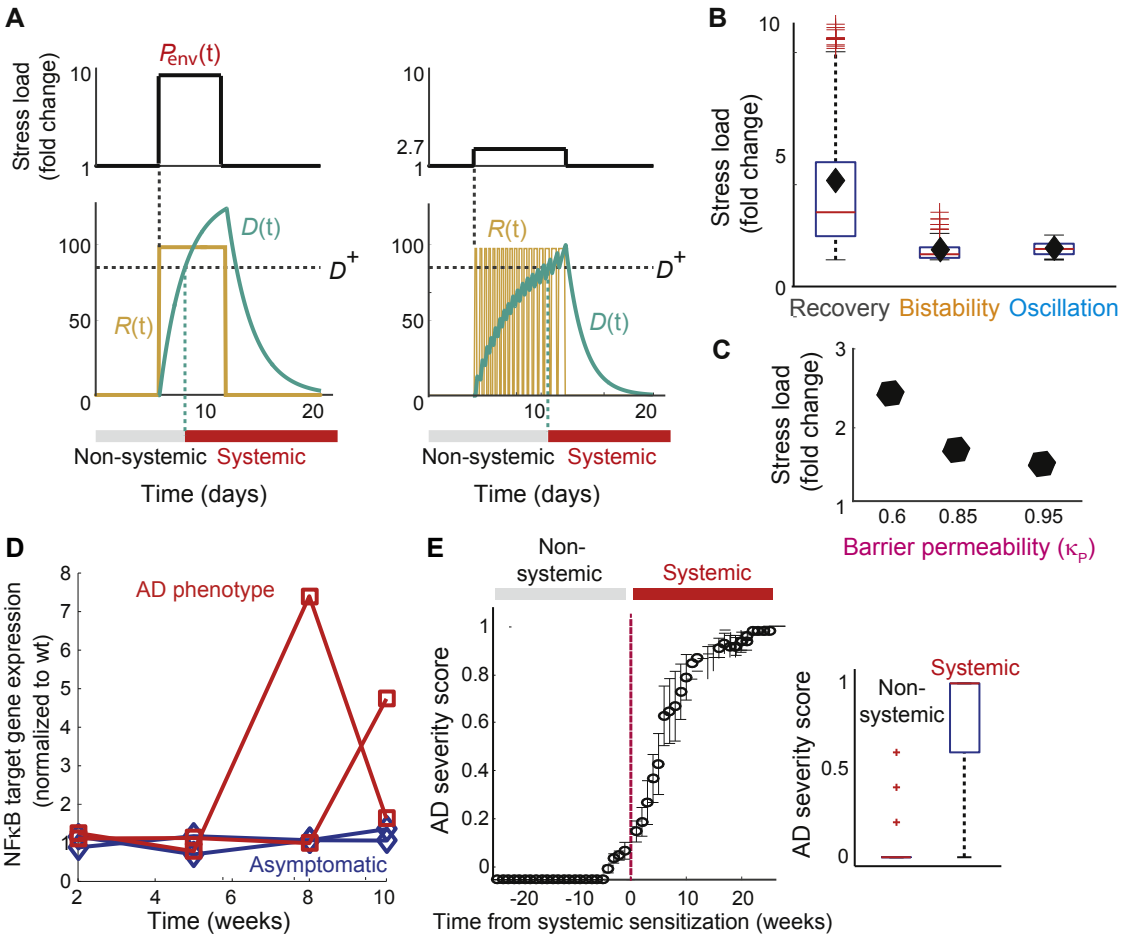

FIG 5. Genetic risk factors increase the susceptibility to environmental stressors in developing systemic T_H2 sensitization. **A,** Transient increases in the environmental stress load can trigger systemic T_H2 sensitization. **B** and **C,** Minimum stress load decreases with genetic risk factors (Fig 5, *B*) in a dose-dependent manner (Fig 5, *C*). **D** and **E,** *Stat3* knockout mice with AD symptoms had higher NF-κB activity (Fig 5, *D*), and the severity of the symptoms increased sharply after T_H2 sensitization (Fig 5, *E*).

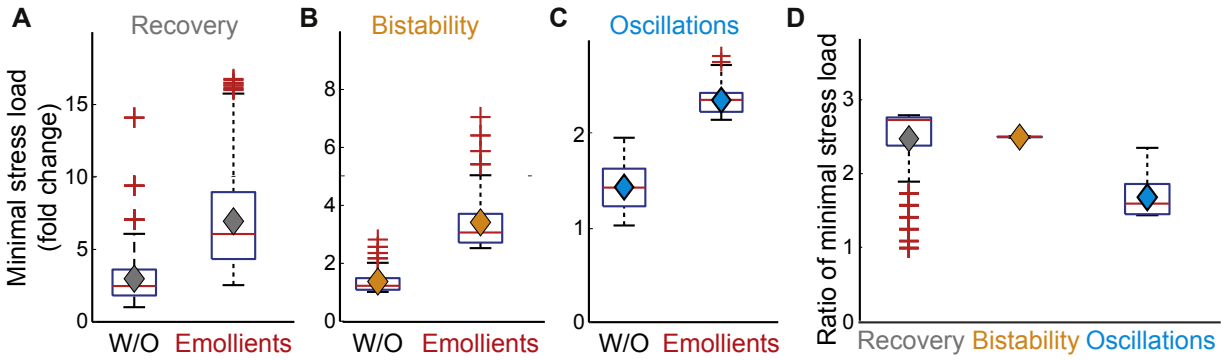

FIG 6. Emollient treatments prevent the progression to severe AD by increasing the computationally predicted minimum stress load required to drive systemic inflammation in *recovery* **(A)**, *bistability* **(B)**, and *oscillation* **(C)** dynamic phenotypes by approximately 2-fold **(D)**.

the minimum stress load required to turn on the *G*-switch (Fig 6). These computational results suggest that topical applications of emollients can counteract the effects of the 2 genetic risk factors investigated in this article (weak barrier integrity and dysregulated immune responses) that asymptomatically increase the susceptibility to environmental stressors and effectively decrease the propensity to develop systemic T_H2 sensitization in response to naturally occurring fluctuations in the environment.

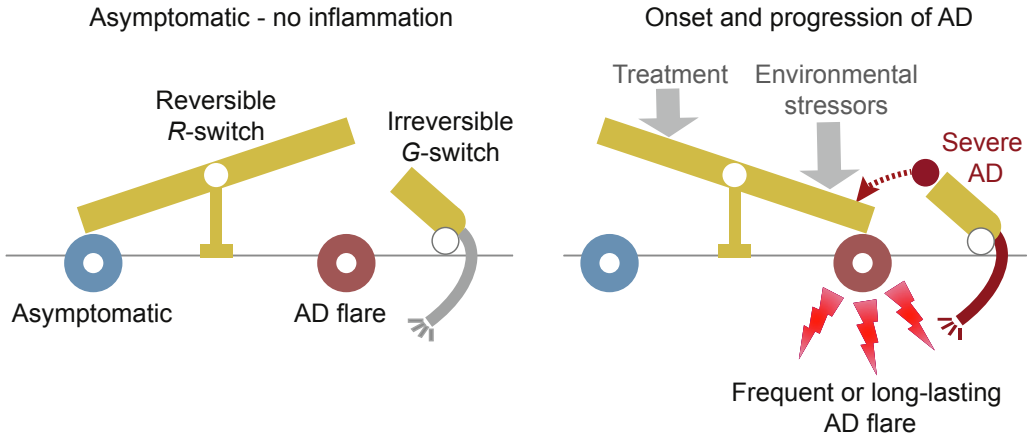

FIG 7. Double-switch mechanism for the onset and progression of AD proposed in this article. Environmental stressors might cause onset of the first reversible switch leading to AD flares, which can be reversed by treatments. Frequent or long-lasting AD flares can trigger the second irreversible switch, resulting in progression to severe AD.

Importantly, our model analysis suggests preventive effects of emollients against the progression of AD through a dynamic interplay between barrier integrity and immune reactions for diverse patient cohorts with different genetic risk factors and not only for those with weak barrier integrity. This prediction is concordant with the results of clinical trials that demonstrated the effective prevention of AD in newborns both with and without filaggrin mutations[26,27] and recently observed preventive effects of emollients in AD mouse models with weak immune responses caused by Jak1 hyperactivation, in which the incidence of AD symptoms was dramatically reduced by regular application of petrolatum on the skin.[65]

DISCUSSION

This article proposes the first mathematical model of AD pathogenesis that reproduces gradual progression from a mostly asymptomatic mild phenotype at its early stage to a severe treatment-resistant form. Our model is a mechanistic representation of the main feedback control structure that regulates the dynamics of AD flare through a relative strength of barrier function and immune responses, corresponding to positive and negative regulation (Fig 1).

We computationally demonstrated that the strengths of the 2 well-known risk factors, dysregulated immune responses and high skin barrier permeability, determine the dynamic phenotypes of AD flare by the *R*-switch and that patients with either of the genetic risk factors might appear asymptomatic initially (Fig 2). Long-lasting or frequent AD flares trigger the activation of the *G*-switch, which underlies the onset of systemic T_H2 sensitization (Fig 3), a hallmark event for progression from mild to clinically severe AD (Fig 4). Our model simulations suggested that the genetic risk factors predispose the carriers to develop a severe AD phenotype, even in response to naturally occurring fluctuations in environmental stressors (Fig 5). These susceptible patient cohorts could benefit from preventive emollient treatments, which increase the threshold stress load that drives systemic T_H2 sensitization (Fig 6).

Our model analysis identified a double switch as a key regulatory motif that determines AD phenotypes of different severity (Fig 4). The first switch (*R*-switch) is responsible for the onset of reversible AD flare, and frequent or long-lasting AD flares can trigger the second switch (*G*-switch), leading to irreversible progression to severe AD through systemic T_H2 sensitization (Fig 7). Description of the AD phenotypes by the status of the *R*- and *G*-switches in our model allows us to uncover and quantitatively investigate the dynamic mechanisms behind worsening or improvement of AD symptoms, which are often evaluated clinically by using an AD score (SCORAD) associated with increased IgE and proinflammatory cytokine levels.[66] The synergetic effects of environmental and genetic risk factors of AD progression determine the dynamics of the *R*- and *G*-switches, which govern a dramatic worsening of AD symptoms through the onset of systemic T_H2 sensitization (*G*-switch on) and could be a target for effective treatment to prevent progression to a severe form of AD.

Our model simulations reproduced several sets of experimental and clinical results, providing plausible mechanistic, quantitative, and coherent explanations for dynamic mechanisms behind the onset, progression, and prevention of AD. This experimentally validated, quantitative, systems-level mathematical framework can be used to uncover possible early biomarkers and investigate new and better treatment options to reverse and control AD symptoms and prevent progression from mild to clinically severe forms of AD. For example, application of predictive control[67] to our model will allow us to computationally design optimal treatment regimens, with minimal treatment times and strengths for effective proactive treatments,[5,63] while reducing the risk of the side effects, such as skin atrophy and barrier damage.[68,69] Our model could also be used to investigate early warning signals[70] to identify asymptomatic but high-risk patient cohorts by their characteristic dynamics in the barrier integrity, such as higher variability (Fig 2, *C*) or a slower recovery (Fig 2, *E*) and identify who might benefit from early treatments that prevent an incipient disease development. Another promising future research includes application of machine learning methods[71] to a large set of clinical data with multiple variables to predict the likelihood of the onset, progression, and prevention of AD. It would also be worth evaluating the stochastic effects of the genetic variants when such data become available.

Consolidating effective treatment strategies for AD will potentially reduce the social and economic burden of this disease by decreasing clinical symptoms and undesired side effects of the treatments that are associated with the advanced stage of AD. The proposed "double-switch" motif provided a coherent explanation of underlying mechanisms behind the dynamic onset, progression, and prevention of AD. The same motif can be found and reveals similar mechanisms underlying the onset, progression, and prevention of other multistage and multifactorial diseases, such as cancers, diabetes, and cardiovascular disease, which are caused by a complex interplay between genetic and environmental factors.

We thank Professor Hywel C. Williams, Professor Michael J. Cork, Dr Simon G. Danby, Professor Mauricio Barahona, and Dr Yuzuru Sato for fruitful discussions and Mr Masao Ukai and Dr Osamu Ohara for data analysis of gene expression levels in *Stat3* knockout mice.

Key messages

- **Mathematical modeling integrating known pathogenic mechanisms discloses that a "double-switch" motif provides a coherent explanation of the dynamic onset, progression, and prevention of AD.**
- **This mathematical model provides a framework to investigate new and better treatments for AD.**

REFERENCES

1. Weidinger S, Novak N. Atopic dermatitis. Lancet 2016;387:1109-22.
2. Bergman JN, Cohen DE, Cooper KD, Cordoro KM, Davis DM, Krol A, et al. Guidelines of care for the management of atopic dermatitis. J Am Acad Dermatol 2014;70:338-51.
3. Spergel JM. Epidemiology of atopic dermatitis and atopic march in children. Immunol Allergy Clin North Am 2010;30:269-80.
4. Bieber T, Akdis C, Lauener R, Traidl-Hoffmann C, Schmid-Grendelmeier P, Schäppi G, et al. Global Allergy Forum and 3rd Davos Declaration 2015: atopic dermatitis/eczema: challenges and opportunities toward precision medicine. Allergy 2016;71:588-92.
5. Wollenberg A, Ehmann LM. Long term treatment concepts and proactive therapy for atopic eczema. Ann Dermatol 2012;24:253-60.
6. Tanaka RJ, Ono M. Skin disease modeling from a mathematical perspective. J Invest Dermatol 2013;133:1472-8.
7. Reynolds NJ. One hundred and twenty-five years and counting: into an era of systems dermatology. Br J Dermatol 2014;171:1279-81.
8. Palmer CN, Irvine AD, Terron-Kwiatkowski A, Zhao Y, Liao H, Lee SP, et al. Common loss-of-function variants of the epidermal barrier protein filaggrin are a major predisposing factor for atopic dermatitis. Nat Genet 2006;38:441-6.
9. Brown SJ, Kroboth K, Sandilands A, Campbell LE, Pohler E, Kezic S, et al. Intragenic copy number variation within filaggrin contributes to the risk of atopic dermatitis with a dose-dependent effect. J Invest Dermatol 2012;132:98-104.
10. Irvine AD, McLean WHI, Leung DYM. Filaggrin mutations associated with skin and allergic diseases. N Engl J Med 2011;365:1315-27.
11. Nemoto-Hasebe I, Akiyama M, Nomura T, Sandilands A, McLean WHI, Shimizu H. Clinical severity correlates with impaired barrier in filaggrin-related eczema. J Invest Dermatol 2009;129:682-9.
12. Paternoster L, Standl M, Waage J, Baurecht H, Hotze M, Strachan DP, et al. Multi-ancestry genome-wide association study of 21,000 cases and 95,000 controls identifies new risk loci for atopic dermatitis. Nat Genet 2015;47:1449-56.
13. McGirt LY, Beck LA. Innate immune defects in atopic dermatitis. J Allergy Clin Immunol 2006;118:202-8.
14. Kezic S, O'Regan GM, Lutter R, Jakasa I, Koster ES, Saunders S, et al. Filaggrin loss-of-function mutations are associated with enhanced expression of IL-1 cytokines in the stratum corneum of patients with atopic dermatitis and in a murine model of filaggrin deficiency. J Allergy Clin Immunol 2012;129:1031-9.e1.
15. Kong HH, Oh J, Deming C, Conlan S, Grice EA, Beatson M, et al. Temporal shifts in the skin microbiome associated with atopic dermatitis disease flares and treatment. Genome Res 2012;22:850-9.
16. Williams MR, Gallo RL. The role of the skin microbiome in atopic dermatitis. Curr Allergy Asthma Rep 2015;15:65.
17. Taïeb A, Seneschal J, Mossalayi MD. Biologics in atopic dermatitis. J Dtsch Dermatol Ges 2012;10:174-8.
18. McAleer M, Irvine AD. The multifunctional role of filaggrin in allergic skin disease. J Allergy Clin Immunol 2013;131:280-91.
19. Cork MJ, Robinson DA, Vasilopoulos Y, Ferguson A, Moustafa M, Macgowan AL, et al. New perspectives on epidermal barrier dysfunction in atopic dermatitis: gene-environment interactions. J Allergy Clin Immunol 2006;118:3-21.
20. Howell MD, Kim BE, Gao P, Grant AV, Boguniewicz M, Debenedetto A, et al. Cytokine modulation of atopic dermatitis filaggrin skin expression. J Allergy Clin Immunol 2007;120:150-5.
21. Fallon PG, Sasaki T, Sandilands A, Campbell LE, Saunders SP, Mangan NE, et al. A homozygous frameshift mutation in the mouse Flg gene facilitates enhanced percutaneous allergen priming. Nat Genet 2009;41:602-8.
22. Scharschmidt TC, Man M-Q, Hatano Y, Crumrine D, Gunathilake R, Sundberg JP, et al. Filaggrin deficiency confers a paracellular barrier abnormality that reduces inflammatory thresholds to irritants and haptens. J Allergy Clin Immunol 2009;124:496-506, e1-6.
23. Kawasaki H, Nagao K, Kubo A, Hata T, Shimizu A, Mizuno H, et al. Altered stratum corneum barrier and enhanced percutaneous immune responses in filaggrin-null mice. J Allergy Clin Immunol 2012;129:1538-46.
24. Domínguez-Hüttinger E, Ono M, Barahona M, Tanaka RJ. Risk factor-dependent dynamics of atopic dermatitis: modelling multi-scale regulation of epithelium homeostasis. Interface Focus 2013;3:20120090.
25. Elias PM, Wakefield JS. Mechanisms of abnormal lamellar body secretion and the dysfunctional skin barrier in patients with atopic dermatitis. J Allergy Clin Immunol 2014;134:781-91.e1.
26. Simpson EL, Chalmers JR, Hanifin JM, Thomas KS, Cork MJ, Mclean WHI, et al. Emollient enhancement of the skin barrier from birth offers effective atopic dermatitis prevention. J Allergy Clin Immunol 2014;134:818-23.
27. Horimukai K, Morita K, Narita M, Kondo M, Kitazawa H. Application of moisturizer to neonates prevents development of atopic dermatitis. J Allergy Clin Immunol 2014;134:824-30.e6.
28. Hoffman DR, Kroll LM, Basehoar A, Reece B, Cunningham CT, Koenig DW. Immediate and extended effects of sodium lauryl sulphate exposure on stratum corneum natural moisturizing factor. Int J Cosmet Sci 2014;36:93-101.
29. Dommisch H, Chung WO, Rohani MG, Williams D, Rangarajan M, Curtis M, et al. Protease-activated receptor 2 mediates human beta-defensin 2 and CC chemokine ligand 20 mRNA expression in response to proteases secreted by *Porphyromonas gingivalis*. Infect Immun 2007;75:4326-33.
30. Yamane H, Zhu J, Paul WE. Independent roles for IL-2 and GATA-3 in stimulating naive CD4+ T cells to generate a Th2-inducing cytokine environment. J Exp Med 2005;202:793-804.
31. Zhang Z, Clarke TB, Weiser JN. Cellular effectors mediating Th17-dependent clearance of pneumococcal colonization in mice. J Clin Invest 2009;119:1899-909.
32. Tanaka RJ, Ono M, Harrington H. Skin barrier homeostasis in atopic dermatitis: feedback regulation of kallikrein activity. PLoS One 2011;6:e19895.
33. Höfer T, Nathansen H, Löhning M, Radbruch A, Heinrich R. GATA-3 transcriptional imprinting in Th2 lymphocytes: a mathematical model. Proc Natl Acad Sci U S A 2002;99:9364-8.
34. Celli S, Day M, Mu AJ, Molina-paris C, Lythe G, Bousso P. How many dendritic cells are required to initiate a T-cell response? Blood 2012;120:3945-8.
35. Chen M, Huang L, Shabier Z, Wang J. Regulation of the lifespan in dendritic cell subsets. Mol Immunol 2007;44:2558-65.
36. Oyarzún D, Chaves M, Hoff-Hoffmeyer-Zlotnik M. Multistability and oscillations in genetic control of metabolism. J Theor Biol 2012;295:139-53.
37. Sano S, Itami S, Takeda K, Tarutani M, Yamaguchi Y, Miura H, et al. Keratinocyte-specific ablation of Stat3 exhibits impaired skin remodeling, but does not affect skin morphogenesis. EMBO J 1999;18:4657-68.
38. Jinnestål CL, Belfrage E, Bäck O, Schmidtchen A, Sonesson A. Skin barrier impairment correlates with cutaneous *Staphylococcus aureus* colonization and sensitization to skin-associated microbial antigens in adult patients with atopic dermatitis. Int J Dermatol 2014;53:27-33.
39. Gittler JK, Shemer A, Suárez-Fariñas M, Fuentes-Duculan J, Gulewicz KJ, Wang CQF, et al. Progressive activation of T(H)2/T(H)22 cytokines and selective epidermal proteins characterizes acute and chronic atopic dermatitis. J Allergy Clin Immunol 2012;130:1344-54.

40. Galli SJ, Tsai M, Piliponsky AM. The development of allergic inflammation. Nature 2008;454:445-54.
41. Hachem J-P, Crumrine D, Fluhr JW, Brown BE, Feingold KR, Elias PM. pH directly regulates epidermal permeability barrier homeostasis, and stratum corneum integrity/cohesion. J Invest Dermatol 2003;121:345-53.
42. Aberg KM, Man M-Q, Gallo RL, Ganz T, Crumrine D, Brown BE, et al. Co-regulation and interdependence of the mammalian epidermal permeability and antimicrobial barriers. J Invest Dermatol 2008;128:917-25.
43. Cenac N, Chin AC, Garcia-Villar R, Salvador-Cartier C, Ferrier L, Vergnolle N, et al. PAR2 activation alters colonic paracellular permeability in mice via IFN-gamma-dependent and -independent pathways. J Physiol 2004;558:913-25.
44. Briot A, Deraison C, Lacroix M, Bonnart C, Robin A, Besson C, et al. Kallikrein 5 induces atopic dermatitis-like lesions through PAR2-mediated thymic stromal lymphopoietin expression in Netherton syndrome. J Exp Med 2009;206:1135-47.
45. Das J, Chen C, Yang L, Cohn L, Ray P, Ray A. A critical role for NF-κ B in Gata3 expression and TH2 differentiation in allergic airway inflammation. Nature 2001; 2:45-50.
46. Duckney P, Wong HK, Serrano J, Yaradou D, Oddos T, Stamatas GN. The role of the skin barrier in modulating the effects of common skin microbial species on the inflammation, differentiation and proliferation status of epidermal keratinocytes. BMC Res Notes 2013;6:474.
47. Yamasaki K, Kanada K, Macleod DT, Borkowski AW, Morizane S, Nakatsuji T, et al. TLR2 expression is increased in rosacea and stimulates enhanced serine protease production by keratinocytes. J Invest Dermatol 2011;131:688-97.
48. Zheng W, Flavell R. The transcription factor GATA-3 is necessary and sufficient for Th2 cytokine gene expression in CD4 T cells. Cell 1997;89:587-96.
49. Leung DYM, Guttman-Yassky E. Deciphering the complexities of atopic dermatitis: shifting paradigms in treatment approaches. J Allergy Clin Immunol 2015; 134:769-79.
50. Sasaki T, Shiohama A, Kubo A, Kawasaki H. A homozygous nonsense mutation in the gene for Tmem79, a component for the lamellar granule secretory system, produces spontaneous eczema in an experimental model of atopic dermatitis. J Allergy Clin Immunol 2013;132:1111-20.e4.
51. Saunders SP, Goh CSM, Brown SJ, Palmer CN, Porter RM, Cole C, et al. Tmem79/Matt is the matted mouse gene and is a predisposing gene for atopic dermatitis in human subjects. J Allergy Clin Immunol 2013;132:1121-9.
52. Hsu AP, Uzel G, Brodsky N, Freeman AF, Demidowich A, Davis J, et al. STAT3 mutations in the hyper-IgE syndrome. N Engl J Med 2007;357:1608-19.
53. Okuma A, Hoshino K, Ohba T, Fukushi S, Aiba S, Akira S, et al. Enhanced apoptosis by disruption of the STAT3-IκB-ζ signaling pathway in epithelial cells induces Sjögren's syndrome-like autoimmune disease. Immunity 2013;38:450-60.
54. Nakamura Y, Oscherwitz J, Cease KB, Chan SM, Muñoz-Planillo R, Hasegawa M, et al. Staphylococcus δ-toxin induces allergic skin disease by activating mast cells. Nature 2013;503:397-401.
55. Man M-Q, Hatano Y, Lee SH, Man M, Chang S, Feingold KR, et al. Characterization of a hapten-induced, murine model with multiple features of atopic dermatitis: structural, immunologic, and biochemical changes following single versus multiple oxazolone challenges. J Invest Dermatol 2008;128:79-86.
56. Imai Y, Yasuda K, Sakaguchi Y, Haneda T, Mizutani H, Yoshimoto T, et al. Skin-specific expression of IL-33 activates group 2 innate lymphoid cells and elicits atopic dermatitis-like inflammation in mice. Proc Natl Acad Sci U S A 2013;110:13921-6.
57. Hams E, Bermingham R, Fallon PG. Macrophage and innate lymphoid cell interplay in the genesis of fibrosis. Front Immunol 2015;6:1-11.
58. Ahmad-Nejad P, Mrabet-Dahbi S, Breuer K, Klotz M, Werfel T, Herz U, et al. The toll-like receptor 2 R753Q polymorphism defines a subgroup of patients with atopic dermatitis having severe phenotype. J Allergy Clin Immunol 2004; 113:565-7.
59. Zasloff M. Antimicrobial peptides of multicellular organisms. Nature 2002;415: 389-95.
60. Sugiura A, Nomura T, Mizuno A, Imokawa G. Reevaluation of the non-lesional dry skin in atopic dermatitis by acute barrier disruption: an abnormal permeability barrier homeostasis with defective processing to generate ceramide. Arch Dermatol Res 2014;306:427-40.
61. Hoffman DR, Kroll LM, Basehoar A, Reece B, Cunningham CT, Koenig DW. Immediate and extended effects of abrasion on stratum corneum natural moisturizing factor. Skin Res Technol 2015;21:366-72.
62. Akira S, Takeda K. Toll-like receptor signalling. Nat Rev Immunol 2004;4: 499-511.
63. Tang TS, Bieber T, Williams HC. Are the concepts of induction of remission and treatment of subclinical inflammation in atopic dermatitis clinically useful? J Allergy Clin Immunol 2014;133:1-12.
64. van Logtestijn MD, Domínguez-Hüttinger E, Stamatas GN, Tanaka RJ. Resistance to water diffusion in the stratum corneum is depth-dependent. PLoS One 2015;10:e0117292.
65. Yasuda T, Fukada T, Nishida K, Nakayama M, Matsuda M, Miura I, et al. Hyperactivation of JAK1 tyrosine kinase induces stepwise, progressive pruritic dermatitis. J Clin Invest 2016;126:2064-76.
66. Vakirlis E, Lazaridou E, Tzellos TG, Gerou S, Chatzidimitriou D, Ioannides D. Investigation of cytokine levels and their association with SCORAD index in adults with acute atopic dermatitis. J Eur Acad Dermatol Venereol 2011;25: 409-16.
67. Hirata Y, di Bernardo M, Bruchovsky N, Aihara K. Hybrid optimal scheduling for intermittent androgen suppression of prostate cancer. Chaos 2010;20:045125.
68. Schoepe S, Schäcke H, May E, Asadullah K. Glucocorticoid therapy-induced skin atrophy. Exp Dermatol 2006;15:406-20.
69. Danby SG, Chittock J, Brown K, Albenali LH, Cork MJ. The effect of tacrolimus compared to betamethasone valerate on the skin barrier in volunteers with quiescent atopic dermatitis. Br J Dermatol 2014;170:914-21.
70. Chen L, Liu R, Liu Z-P, Li M, Aihara K. Detecting early-warning signals for sudden deterioration of complex diseases by dynamical network biomarkers. Sci Rep 2012;2:342.
71. Shouval R, Bondi O, Mishan H, Shimoni A, Unger R, Nagler AG. A data-mining approach in SCT. Bone Marrow Transplant 2014;49:332-7.

METHODS

LPS challenges and histologic evaluation of epidermis-specific *Stat3* knockout mice

We backcrossed the keratinocyte-specific *Stat*3 knockout *(Stat3$^{f/f}$)* mice on a B6X129 mixed background with a B6 background. We applied 3 intradermal injections with an interval of a week of sterile PBS with 0.1% dimethyl sulfoxide, with and without LPS (10 μg), to the ears of asymptomatic keratinocyte-specific *Stat3$^{f/f}$* mice with a B6 background (8-9 weeks). Two days after the last injection, ears were fixed with paraformaldehyde (4%) and frozen in OCT compound (Sakura Finetek Japan, Tokyo, Japan). Five-micrometer sections were taken with a cryostat (Leica, Wetzlar, Germany) and fixed onto slide glasses. After retrieval with Target Retrieval Solution (Agilent Technologies, Santa Clara, Calif) and permeabilization (0.1% Trirtonx-100), the sections were stained with hematoxylin and eosin.

Minimum flare time and minimum relaxation time to trigger systemic T_H2 sensitization

The solution of Equation 1c,

$$\frac{D(t)}{dt} = \kappa_{DC} R(t) - \delta_D D(t)$$

is described by

$$D(t) = e^{-\delta_D (t-t_0)} D(t_0) + \int_{t_0}^{t} e^{-\delta_D (t-\tau)} \kappa_{DC} R(\tau) d\tau, \tag{E1}$$

where the integral is defined over each time segment, on which $R(t)$ is continuously defined, either by $R(t) = R_{on}$ for the duration of a flare time (t_{on}) or by $R(t) = R_{off} = 0$ for the duration of a relaxation time (t_{off}). Note that the steady-state value (D_{ss}) of $D(t)$ while $R(t) = R_{on}$ is obtained by $D_{ss} = \frac{\kappa_{DC} R_{on}}{\delta_D}$. The period of the R-spike is denoted by $T = t_{on} + t_{off}$.

To determine the dynamics of $D(t)$, we derive $D(t_k)$ and $D(T_k)$ ($k = 1,2,\ldots$), where t_k and T_k denote the time when the k-th spike of $R(t) = R_{on}$ starts and the time when the k-th spike ends, respectively. We define $t_1 = 0$ and $D(t_1) = 0$. $D(t)$ decreases during $T_k \le t \le t_{k+1}$ when $R(t) = R_{off} = 0$ and reaches $D(t_{k+1}) = e^{-\delta_D t_{off}} D(T_k)$, whereas it increases during $t_k \le t \le T_k$ with $R(t) = R_{on}$ and achieves

$$\begin{aligned} D(T_k) &= e^{-\delta_D t_{on}} D(t_k) + \kappa_{DC} R_{on} \int_{t_k}^{T_k} e^{-\delta_D (T_k - \tau)} d\tau \\ &= e^{-\delta_D t_{on}} D(t_k) + \kappa_{DC} R_{on} e^{-\delta_D T_k} \int_{t_k}^{T_k} e^{\delta_D \tau} d\tau \\ &= e^{-\delta_D t_{on}} D(t_k) + D_{ss} \left(1 - e^{-\delta_D t_{on}}\right). \end{aligned} \tag{E2}$$

Because $D(t_1) = 0$ for $t_1 = 0$, we have $D(T_1) = D_{ss}(1 - e^{-\delta_D t_{on}})$ and

$$\begin{aligned} D(T_k) &= e^{-\delta_D t_{on}} e^{-\delta_D t_{off}} D(T_{k-1}) + D_{ss}\left(1 - e^{-\delta_D t_{on}}\right) = \\ &\quad e^{-\delta_D T} D(T_{k-1}) + D_{ss}\left(1 - e^{-\delta_D t_{on}}\right), \quad k = 2, 3, \ldots. \end{aligned}$$

Therefore $D(T_k)$ is described as

$$D(T_k) = D_{ss}\left(1 - e^{-\delta_D t_{on}}\right) \sum_{i=0}^{k-1} e^{-i\delta_D T}, \tag{E3}$$

which converges to

$$D(T_\infty) = \lim_{k \to \infty} D(T_k) = D_{ss}\left(1 - e^{-\delta_D t_{on}}\right) \frac{1}{1 - e^{-\delta_D T}}. \tag{E4}$$

The minimum flare time, t^*_{on}, for a single pulse of $R(t) = R_{on}$ to trigger systemic T_H2 sensitization is analytically obtained from the corresponding solution $D(t) = \int_0^t e^{-\delta_D (t-\tau)} \kappa_{DC} R(\tau) d\tau = D_{ss}(1 - e^{-\delta_D t})$ of Equation E1.

Solving $D(t^*_{on}) = D^+$ leads to

$$t^*_{on} = -\frac{\ln\left(1 - \frac{D^+}{D_{ss}}\right)}{\delta_D}. \tag{E5}$$

The minimum relaxation time, t^*_{off}, for a periodic R-spike with a fixed t_{on} to trigger systemic T_H2 sensitization is analytically obtained by solving $D(T_\infty) = D^+$ as

$$t^*_{off} = -\left[t_{on} + \frac{1}{\delta_D} \ln\left\{1 - \frac{D_{ss}}{D^+}\left(1 - e^{-\delta_D t_{on}}\right)\right\}\right]. \tag{E6}$$

Note that the solution in Equation E6 exists if $1 - \frac{D_{ss}}{D^+}(1 - e^{-\delta_D t_{on}}) > 0$ and $t_{on} + \frac{1}{\delta_D} \ln\left\{1 - \frac{D_{ss}}{D^+}(1 - e^{-\delta_D t_{on}})\right\} < 0$. These conditions are equivalent to

$$t_{on} < -\frac{1}{\delta_D} \ln\left(1 - \frac{D^+}{D_{ss}}\right) = t^*_{on} \quad \text{and} \quad D^+ < D_{ss}.$$

OVA patch challenges and measurement of IgE levels in *Stat3* knockout mice

We applied an OVA-soaked patch (1 mg/mL in 100 μL) to the shaved back skin of the 8- to 9-week-old mice (3 WT and 4 epidermis-specific *Stat3* knockout mice) 4 times at a week interval between individual applications. We measured the level of OVA-specific IgE titer in the serum by using a sandwich ELISA a week after the last OVA challenge. Briefly, serum was applied on the plastic plate coated with captured antibody for IgE. After washing, the plate was probed with the biotinylated specific OVA antibody for the cytokines and horseradish peroxidase–conjugated streptavidin (Zymed, San Francisco, Calif) and developed with 2,2′-azino-bis (3-ethylbenzthiazoline-6-sulfonic acid; Kirkegaard & Perry Laboratories, Gaithersburg, Md). The 405-nm absorbance was measured by using a spectrophotometer (Bio-Rad Laboratories, Hercules, Calif).

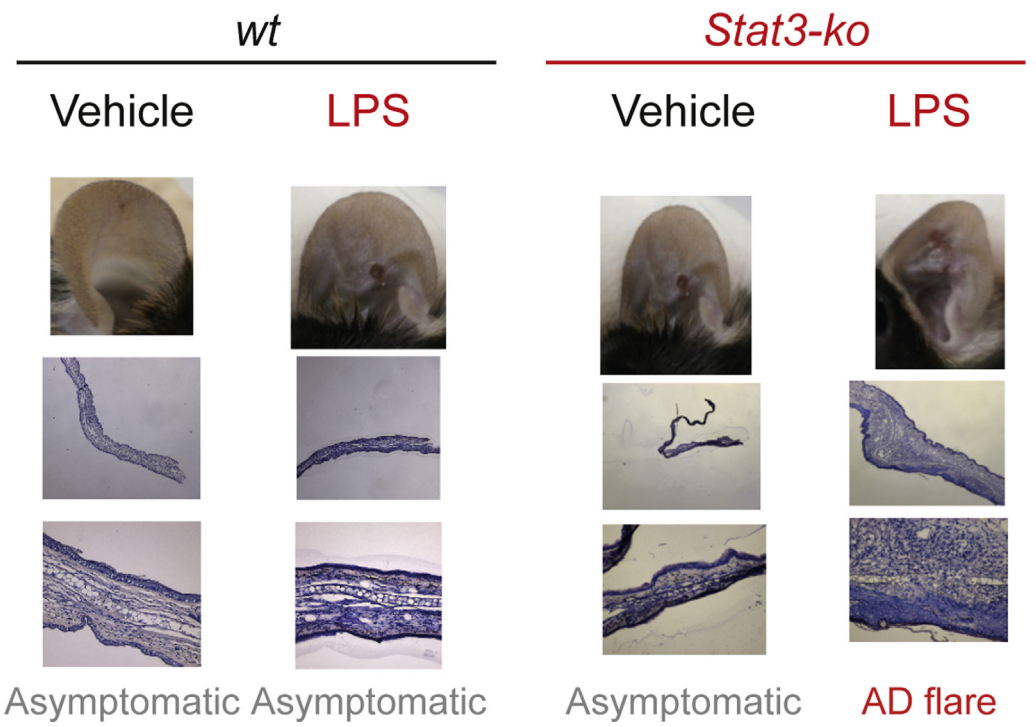

FIG E1. Induction of AD symptoms by environmental triggers (LPS) in a *Stat3* knockout mouse model of AD.

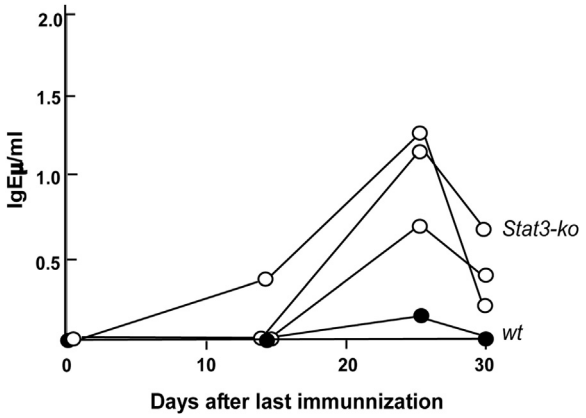

FIG E2. Constitutive environmental challenges with OVA result in an increase in IgE levels in *Stat3* knockout mice (n = 3) but not in WT (n = 1) mice.

TABLE E1. Experimental data on IgE levels and AD severity scores in *Stat3* knockout mice (Fig 5, *E*)

	Time (wk)																																								
	0	11	12	13	14	15	16	17	18	19	20	21	22	23	24	25	26	27	28	29	30	31	32	33	34	35	36	37	38	39	40	41	42	43	44	45
Mouse identifier	IgE levels																																								
5	0				0						0.4	0.4	0.3	0	1.5	0.2	0.4	17	2.6								8.1														
1	0		3.1		2.4		8.7		1.5	4	63	43	53	15	92	39	18	36									4.4														
2	0				6.6.2 E+00		20		12			16																4.8														
4	0				0.3		2.5		1.6	1.5	18		6.3	9.2	28	9.7	5.6	17		29		4.1		1.9	2.3		35	38		20											
110	0			1.1		0					0.3	0.9	5.7	6.8														4.8													
101	0			0		0						1.5	1.9	2.3	1.2	8.5	3.1	2.3	3.6	2	4.7	1.9	0.5		0.4	0.4		12		2.7	12									
104	0			0				0.8		1.6	0.4																	2												
106	0			0		0.4		15		17																		4.5												
108	0			0		0				1.3	0.5																													
97	0					0								0.4	0.6			0	0.4	0	0	0.1	0	0	0	18				0.1			0			0				
96	0					0.7				25		49	40																42											
	Severity of AD symptoms																																								
5	0	0	0	0	0	0	0	0	0	0	0	0	0	0	0	0	0	0	0	0	1	1	1	2	2	5	5	5	5	5	5	5	5	5	5	5	5	5	5	5
1	0	0	0	0	0	0	0	1	1	1	1	1	1	3	4	5	5	5	4	5	5	5	5	5	5	5	5	5	5	5	5	5	5	5	5	5	5	5	5	5
2	0	0	0	0	0	0	0	1	2	3	3	4	4	5	5	5	5	5	4	5	5	5	5	5	5	5	5	5	5	5	5	5	5	5	5	5	5	5	5	5
4	0	0	0	0	0	0	0	0	1	1	1	1	2	3	4	4	4	4	3	3	3	3	5	5	5	5	5	5	4	4	4	4	4	5	5	5	5	5	5	5
110	0	0	0	0	0	0	0	0	0	0	0	0	1	2	3	4	4	4	4	5	4	4	5	5	5	5	5	5	5	5	5	5	5	5	5	5	5	5	5	5
101	0	0	0	0	0	0	0	0	0	0	0	0	0	0	0	0	0	2	1	1	2	2	3	3	3	3	3	3	3	4	4	4	4	5	5	4	5	5	5	5
104	0	0	0	0	0	0	0	2	2	2	2	3	4	5	5	5	5	5	5	5	5	5	5	5	5	5	5	5	5	5	5	5	5	5	5	5	5	5	5	5
106	0	0	0	0	1	1	1	2	2	2	2	2	5	5	5	5	5	5	5	5	5	5	5	5	5	5	5	5	5	5	5	5	5	5	5	5	5	5	5	5
108	0	0	0	0	0	0	0	0	0	1	1	2	2	2	2	2	2	2	2	2	2	2	2	2	2	2	2	2	2	3	3	3	3	3	3	3	3	3	3	3
97	0	0	0	0	0	0	0	0	0	0	0	0	0	0	0	0	0	0	0	0	0	0	0	0	0	0	0	0	0	0	2	2	2	3	4	5	5	5	5	5
96	0	0	0	0	0	2	2	2	3	3	4	5	5	5	5	5	5	5	5	5	5	5	5	5	5	5	5	5	5	5	5	5	5	5	5	5	5	5	5	5

TABLE E2. Experimental data on the dynamic expression of 11 NF-kB target genes (Fig 5, *D*)

Time (wk)	2	5	8	10	
	Control - mouse 1				
NF-κB target gene	**C1_2w**	**C1_5w**	**C1_8w**	**C1_10w**	
Bcl2	1.49096	1.00037	1.60742	2.25852	
Ddx26b	12.1838	12.8617	13.7913	18.9728	
Gadd45b	10.2747	10.4486	24.0344	14.2288	
Icam1	11.1869	8.10447	14.1105	15.6618	
Icam2	5.67296	2.29207	2.83728	1.86459	
Icam4	0.479092	0.0986578	0.258129	0.995197	
Icam5	0.145468	0.0998525	0.566053	0.553987	
Il1b	13.7828	0.55531	2.04485	0.373441	
Tnf	5.23604	1.47033	3.12033	1.28542	
Traf1	1.04792	0.686619	0.826949	1.31927	
Traf2	7.73797	7.76872	9.09156	9.28874	
Vcam1	12.4412	4.71144	4.69602	4.27077	
Mean NF-κB target gene expression (control mouse 1)	6.806650833	4.1748449	6.4153993	5.9227779	
	Control: mouse 2				
NF-κB target gene	**C2_2w**	**C2_5w**	**C2_8w**	**C2_10w**	
Bcl2	1.46856	2.09932	1.73659	1.02413	
Ddx26b	12.834	20.853	17.0093	13.4294	
Gadd45b	15.0294	16.3331	14.8715	8.53494	
Icam1	9.57862	16.4514	11.0136	8.20556	
Icam2	5.50534	2.59863	3.39916	2.74231	
Icam4	0.667817	0.403192	0.21096	0.348492	
Icam5	0.394278	0.775341	0.186825	0.198401	
Il1b	1.39219	0.806906	1.97903	1.03526	
Tnf	6.37709	3.32492	4.4016	1.55811	
Traf1	1.20497	1.73708	1.04871	0.866203	
Traf2	7.87773	9.92028	7.88133	8.17552	
Vcam1	11.5451	4.96892	6.38359	4.6591	
Mean NF-κB target gene expression (C mouse 2)	6.156257917	6.6893408	5.8435163	4.2314522	
Mean NF-κB target gene expression of control mice (for normalization)	6.48145438	5.4320928	6.129458	5.077115	Data used for normalization
	***Stat3* knockout asymptomatic: mouse 1**				
NF-κB target gene	**H1_2w**	**H1_5w**	**H1_8w**	**H1_10w**	
Bcl2	1.84859	1.37405	2.22196	2.5455	
Ddx26b	24.3847	14.5103	18.9545	25.2859	
Gadd45b	15.0237	13.2383	17.7276	16.8651	
Icam1	6.02257	8.67721	13.1487	9.98603	
Icam2	7.9638	4.53143	3.22786	3.20087	
Icam4	0.103169	0.332223	0.704791	0.39274	
Icam5	0.208837	0.201748	0.653882	0.583823	
Il1b	0.580702	0.457103	3.96702	1.136	
Tnf	2.92136	1.35334	3.07331	1.51206	
Traf1	1.1625	0.770714	2.77694	1.43174	
Traf2	5.0872	6.73656	9.53535	8.99125	
Vcam1	6.78865	6.65325	6.23863	3.40321	
Mean NF-κB target gene expression (asymptomatic mouse 1)	6.0079815	4.903019	6.8525453	6.2778519	
Normalized mean NF-κB target gene expression asymptomatic mouse 1 (to control)	0.926949594	0.9026022	1.1179692	1.2364998	Plotted data

(Continued)

TABLE E2. *(Continued)*

	***Stat3* knockout asymptomatic: mouse 2**				
NF-κB target gene	**H2_2w**	**H2_5w**	**H2_8w**	**H2_10w**	
Bcl2	2.41956	1.23529	2.10121	1.68742	
Ddx26b	21.5093	14.3954	24.1115	19.1582	
Gadd45b	24.2009	9.00596	17.8458	16.9307	
Icam1	11.1511	10.0336	8.47175	10.8174	
Icam2	5.5099	3.32845	3.42015	3.09949	
Icam4	0.198705	0.211489	0.702098	0.381764	
Icam5	0.251389	0.267563	0.24871	0.434685	
Il1b	1.24271	0.617243	1.27338	1.35296	
Tnf	3.55363	2.06624	2.30199	1.39078	
Traf1	2.17314	0.887801	1.51243	0.801295	
Traf2	8.19833	6.95227	7.6482	8.33978	
Vcam1	5.53173	7.30719	5.17613	4.49481	
Mean NF-κB target gene expression (asymptomatic mouse 2)	7.1616995	4.6923747	6.2344457	5.7407737	
Normalized mean NF-κB target gene expression asymptomatic mouse 2 (to control)	1.10495254	0.8638245	1.017128	1.130716	Plotted data
	***Stat3* knockout symptomatic: mouse 1**				
NF-κB target gene	**D1_2w**	**D1_5w**	**D1_8w**	**D1_10w**	
Bcl2	2.91098	1.93891	2.06153	1.11461	
Ddx26b	23.895	10.6448	23.4599	7.08725	
Gadd45b	23.3722	12.3531	23.933	22.7247	
Icam1	13.4452	11.8311	8.9785	14.4459	
Icam2	5.69212	2.91948	2.05203	5.2818	
Icam4	0.404001	0.634164	0.491453	0.418676	
Icam5	0.511117	0.504306	0.426347	0.282497	
Il1b	0.606394	0.339951	2.10759	256.125	
Tnf	3.45202	0.810098	1.49973	3.95179	
Traf1	1.84768	1.53122	1.37278	3.14507	
Traf2	8.74087	7.9771	7.52432	9.33925	
Vcam1	6.08137	4.96439	2.45665	12.669	
Mean NF-κB target gene expression (symptomatic mouse 1)	7.579912667	4.7040516	6.3636525	28.048795	
Normalized mean NF-κB target gene expression symptomatic mouse 1 (to control)	1.169477131	0.8659741	1.0382081	5.5245538	Plotted data
	***Stat3* knockout symptomatic: mouse 2**				
NF-κB target gene	**D2_2w**	**D2_5w**	**D2_8w**	**D2_10w**	
Bcl2	1.97776	1.43348	1.71809	2.27594	
Ddx26b	22.1149	16.3475	15.2385	24.9703	
Gadd45b	24.0066	14.7206	36.3763	21.2089	
Icam1	12.1641	10.1451	29.7421	8.29952	
Icam2	4.82864	2.51071	6.82758	2.72525	
Icam4	0.935281	0.570237	0.391841	0.548891	
Icam5	0.420714	0.468928	0.272653	0.572899	
Il1b	0.974882	0.534944	390.257	9.78346	
Tnf	8.10515	1.55804	7.49432	1.09071	
Traf1	1.51537	1.3465	9.57717	0.795847	
Traf2	8.73212	8.87655	10.819	8.11274	
Vcam1	6.86094	4.31381	10.1108	2.56689	
Mean NF-κB target gene expression (symptomatic mouse 2)	7.71970475	5.2355333	43.235446	6.9126123	
Normalized mean NF-κB target gene expression symptomatic mouse 2 (to control)	1.19104514	0.9638151	7.053715	1.361524	Plotted data
Mean normalized NF-κB asymptomatic	1.01595107	0.8832133	1.067549	1.183608	
Mean normalized NF-κB symptomatic	1.18026114	0.9148946	4.045961	3.443039	

TABLE E3. Experimental data on the IgE levels in serum after application of the OVA-soaked patch (Fig E2)

	Time (d)			
Mice	0	13	25	30
WT 1	0	0	0.15	0
Knockout 1	0	0.4	1.3	0.2
Knockout 2	0	0	1.2	0.7
Knockout 3	0	0	0.7	0.25